



Broadband dielectric dispersion (20 Hz–1 GHz) and relaxation, crystalline structure, and thermal characterization of PVDF/PMMA blend films

Naresh Kumar¹ · R. J. Sengwa¹

Received: 19 July 2022 / Revised: 21 October 2022 / Accepted: 4 December 2022 /
Published online: 15 December 2022

© The Author(s), under exclusive licence to Springer-Verlag GmbH Germany, part of Springer Nature 2022

Abstract

Polymer blend films consisted of poly(vinylidene fluoride) (PVDF) and poly(methyl methacrylate) (PMMA) (compositional ratios of PVDF/PMMA = 100/0, 80/20, 60/40, 40/60, 20/80, and 0/100 wt/wt%) were prepared by solution casting method. These PVDF/PMMA blend films were characterized by employing an X-ray diffractometer, Fourier transform infrared spectroscopy, scanning electron microscope, differential scanning calorimeter, and broadband dielectric relaxation spectroscopy. The PVDF crystal phases formed in these polymer blends were explained and their crystallite sizes, degree of crystallinity, and melting temperatures were determined. The dielectric dispersion study over the broadband frequency range of 20 Hz–1 GHz confirmed the decrease in dielectric permittivity with increased frequency of the applied harmonic electric field and it changed anomalously when the PVDF/PMMA blend compositional ratio varied. Dielectric loss tangent spectra illustrated the blend composition-dependent PVDF chain segmental relaxation process in these polymer blends which appeared in the radio frequency region. The alternating current electrical conductivity spectra revealed the increase in conductivity with increased frequency, and at a fixed frequency, the conductivity showed a variation in one order of magnitude with the variation in the blend composition ratio over the entire range. The experimental results highlighted that these PVDF/PMMA blend films could be used as frequency tunable dielectrics and insulating materials for advances in next-generation flexible device technologies.

Keywords PVDF/PMMA blend · PVDF crystals · Thermal properties · Dielectric properties · Electrical conductivity

✉ R. J. Sengwa
rjsengwa@rediffmail.com; rjs.ph@jnvu.edu.in

¹ Dielectric Research Laboratory, Department of Physics, Jai Narain Vyas University, Jodhpur 342 005, India

Introduction

In recent years, flexible-type polymeric dielectric materials, having poly(vinylidene fluoride) (PVDF) as one of the constituents, attracted considerable attention in research due to their promising properties suitable for widespread technological applications [1–5]. The polymorphs of semicrystalline PVDF matrix and this matrix-based hybrid nanocomposites play an important role to be used as a dielectric, electric insulator, and functional materials in the design and development of the desired dimension advanced flexible-type energy generator and storage devices [2, 5]. Furthermore, the polymeric materials that have controllable dielectric and electrical insulation properties over wide-range radio frequencies are credited to enormous industrial and technological applications, especially in the development of tunable capacitors, electromagnetic interference shielders, high-performance radio frequency antennas, microwave integrated circuits, etc. [6–11]. However, to date, limited work is available on the dielectric properties of polymers, their blends, and nanocomposites over the broadband radio frequency range from 1 MHz to 1 GHz [7, 8, 10–13] which is more needed and to be carried out to meet the industrial demands for advances in high-frequency device technologies. Among the synthetic polymers, poly(vinylidene fluoride) (PVDF), poly(methyl methacrylate) (PMMA), poly(ethylene oxide) (PEO), polyaniline (PANI), polypyrrole (PPy), polyamide (PA), polyacrylonitrile (PAN), polyethylene terephthalate (PET), poly(tetrafluoroethylene) (PTFE), polyacrylate (PC), poly(vinyl alcohol) (PVA), etc., are largely investigated to be used as dielectrics for the advances in flexible types variety of electronic and electrical devices [1, 3, 4, 10, 11, 14–16].

The PVDF is credited as an electroactive polymer due to its appreciable thermoplastic and electroactive properties [2, 3, 5]. It is extensively used as a dielectric material for energy storage because of its several useful properties like high mechanical strength, lightweight, good thermal stability, elevated dielectric strength, appropriate dielectric properties, good chemical inertness, high plasticity, sensible optical transparency, and also piezoelectric and pyroelectric properties [2, 5, 17–21]. In particular, the semicrystalline PVDF matrix may exist in a variety of polar and non-polar crystal phases denoted by α , β , γ , δ , and ϵ [2, 3]. Among these polymorphs, the α -phase is non-polar and most commonly observed in the PVDF matrix-based films when prepared by all the established methods, whereas the polar β -phase is highly appreciated for technological advances, and therefore, it is created by various treatments of the prepared films (e.g. mechanical, electrical, thermal, etc.) [2, 3, 5, 21, 22]. The polar γ -phase in the solution-cast PVDF film can be introduced by its annealing at an appropriate high temperature [22]. Detailed characteristics of a unit cell, conformation, and dipole moment of these polymorphs and their formation in PVDF are summarized in the review articles [3, 22].

The α -phase of PVDF material exhibits low-dielectric permittivity due to its non-polar character. A thermodynamically stable electroactive polar β -phase exhibits high polarizability due to effectively arranged dipoles of repeat units

(CH₂–CF₂) that are oriented in a parallel direction to the applied harmonic alternating current (AC) electric field, and hence resulted in high dielectric permittivity as compared to the other crystal phases of the PVDF matrix [2, 17, 20]. The β -phase credited appreciable dielectric, piezo-, pyro-, and ferroelectric characteristics of PVDF matrix which have a high significance in the fabrication of advanced energy storage and harvesting devices (viz. supercapacitors, nanogenerators, actuators, transducers, sensors, and high energy rechargeable batteries) [3, 5, 8, 17–24]. A literature survey revealed that the dielectric permittivity of the PVDF film at low frequencies and ambient temperature may be in the range of 4–12 depending on the relative amount of various crystal phases developed in the prepared film and additionally its state-of-the-art treatments with mechanical stretching, electrospinning, irradiating, etc. [2, 3, 5, 20–22]. For the investigation of PVDF material properties, its films are formed through various established methods like melting under high pressure, electrospinning, heat-controlled spin-coating, and solution casting using the solvents like dimethylformamide or dimethylacetamide [2, 3, 5, 13, 21, 22].

In the last decade, numerous studies established that the structural, thermal, optical, and dielectric properties of a PVDF matrix can also be modified and tailored with the state-of-the-art by blending with non-polar or polar polymers and further making its matrix-based nanocomposites with a variety of nanofillers through suitable film fabrication routes [12, 13, 18, 19, 21, 23–26]. Previous studies also concluded that the PVDF forms miscible blends over the entire composition range with some of the polymers such as poly(methyl methacrylate) (PMMA), polyacrylate (PC), chitosan, and polyketone which is a result of heterogeneous interactions developed between the functional fluorocarbon group of the PVDF and the carbonyl groups of these blended polymers [18, 25, 27–29]. The polymer blends consisted of semicrystalline PVDF and amorphous PMMA are immensely studied for confirmation of the blend miscibility, crystallization, and dielectric polarization [23, 24, 28, 30–32]. The PMMA is important transparent plexiglass of low permittivity over a wide frequency and temperature range [11, 33–36]. Therefore, it is frequently used as a dielectric in the preparation of microelectronic devices and also the multi-functional composites for their promising electronic and optoelectronic applications [33–36]. But high brittleness of the PMMA film is one of the major drawbacks to the realization of dimensional design flexibility of modern electronic devices [11, 25, 33–36]. In contrast to the PMMA film, the PVDF film bears appreciable flexibility, and therefore, the designed PVDF/PMMA blend film can serve as a better flexible dielectric and insulating material for advances in polymer technologies. With this point of view, a detailed study of varying compositional ratio engineered PVDF/PMMA blend films is needed over a broadband frequency range to highlight their possible dielectric applications in next-generation microelectronic devices.

Therefore, in consideration of above-mentioned facts, the present study deals with the detailed characterization of varying composition PVDF/PMMA blend films. For this purpose, different compositional ratios PVDF/PMMA blend films (i.e. PVDF/PMMA = 100/0, 80/20, 60/40, 40/60, 20/80, 0/100 wt/wt%) were prepared by the solution casting method. These films are characterized to their morphological, structural, thermal, dielectric, and electrical properties by employing

advanced techniques. The dielectric and electrical measurements are performed over nine orders of magnitude broadband frequency range which is its kind of the first study on these polymer blend materials. The in-depth analysis of the experimental data with the composition variation in the PVDF/PMMA blends revealed some structure-property relationships and also explained the suitability of these polymer blend films for polymer engineering and technologies-based next-generation flexible devices.

Experimental

Materials

The powder samples of PVDF (average molecular weight $M_w \sim 5.34 \times 10^5$ g/mol) from Sigma-Aldrich, France, and the PMMA (average molecular weight $M_w \sim 3.50 \times 10^5$ g/mol) from Sigma-Aldrich, Germany were used for the preparation of PVDF/PMMA blend films. *N,N*-dimethyl formamide (DMF) for HPLC and UV spectroscopy grade from Loba Chemie, India was used as a common solvent for the PVDF and the PVDF/PMMA blend powders, whereas tetrahydrofuran (THF) for HPLC grade from SD Fine-Chem Limited, India was used as a solvent for pure PMMA powder.

Preparation of PVDF/PMMA blend films

The PVDF/PMMA blend films of different compositional ratios (i.e. PVDF/PMMA = 100/0, 80/20, 60/40, 40/60, 20/80, 0/100 wt/wt%) were prepared by solution casting film preparation method. Initially, the required amounts of PVDF and PMMA powders for a fixed compositional ratio were taken into the stoppered conical glass bottle for the preparation of the blend solution in the DMF solvent. The homogeneous solution of the PVDF/PMMA blend was obtained in DMF with a continuous magnetic bar stirring at 500 rpm and simultaneous heating at 60 °C using a thermostated hot plate magnetic bar stirrer. Different compositional ratios of PVDF/PMMA blend solutions were prepared by the same procedure in separate glass bottles. After that, these homogeneous polymeric solutions were cast onto the glass Petri dishes and heated at about 70 °C on the thermostated hot plate till the DMF solvent was completely evaporated and turned the dissolved polymers into the films. The pure PMMA film was formed by casting its solution at room temperature, which was prepared in THF solvent. These solution-cast prepared films of PVDF/PMMA blend and also the pristine PVDF and PMMA were dried overnight at 45 °C in a vacuum oven to remove the solvent traces.

Characterization techniques

The microimages of the pure PVDF film, PVDF/PMMA (80/20 wt/wt%) blend film, and the pure PMMA film were recorded with Zeiss EVO 18 scanning electron microscope (SEM) at 10 μm scale and 1.0 KX magnification.

The X-ray diffraction (XRD) patterns of all the polymeric films were recorded by using an X'pert Pro multipurpose powder diffractometer (MPD) of Malvern PANalytical, The Netherlands. The X-ray radiations of wavelength 1.5406 \AA were generated from Cu- K_{α} target of the X-ray tube biasing it at the voltage of 45 kV with a current of 40 mA. The XRD patterns of the films were recorded by fixing the films, one after another, on the power sample holder. These XRD measurements of the films at ambient temperature were performed in the reflection mode operation of the diffractometer with an angular sweep speed of 0.05 deg/s over the 2θ range from 10° to 42°.

The Fourier transform infrared (FTIR) transmittance spectra of the films in the wavenumber range from 650 to 4000 cm^{-1} were recorded in attenuated total reflectance (ATR) mode by employing the FTIR spectrometer (Agilent Technologies; Cary 630).

The thermograms of the samples were recorded in the temperature range from 55 to 200 °C with a heating rate of 10 °C/min by employing the differential scanning calorimeter (DSC) of Netzsch (Polyma 214), Germany. For the DSC measurements, the required amount of the sample (about 7 mg) was filled into an aluminium pan covered with a pierced lid and it was placed into the Arena[®] furnace having a nitrogen flow at a rate of 40 mL/min. These DSC measurements were controlled with Netzsch Proteus[®] software.

The frequency-dependent electrical measurements (capacitance C_p , resistance R_p , and dielectric dissipation factor D (dielectric loss angle tangent $\tan\delta$)) of the polymer films were carried out using the precision inductance–capacitance–resistance (LCR) meter of 1-V signal amplitude with frequency variation in the range from 20 Hz to 1 MHz. The precision LCR meter of Agilent Technologies, Model: 4284A, and a parallel circular plates solid dielectric test fixture of 38 mm diameter active electrode (Model: 16451B) were used for these electrical measurements. The frequency-dependent complex permittivity $\varepsilon^*(\omega) = \varepsilon' - \varepsilon''$ values of the samples were determined from the measured electrical quantities C_p , R_p , and D . The real part of permittivity ε' and dielectric loss tangent ($\tan\delta = \varepsilon''/\varepsilon'$) in the frequency range of 1 MHz–1 GHz of the PVDF/PMMA blend films were measured by employing radio frequencies impedance/material analyzer (IMA of Keysight Technologies, Model: E4991B, equipped with a solid test fixture of 15 mm diameter electrodes Model: 16453A). The test fixture was calibrated with short, open, and standard load (teflon), before the sample measurements. Thereafter, the ε' and $\tan\delta$ values of the samples, appropriately mounted between the electrodes were measured directly by sweeping the frequency from 1 MHz to 1 GHz which was controlled by material measurement firmware of Keysight Technologies (E499B-002). The dielectric test fixtures used with the LCR meter and IMA equipment have a special design that meets the ASTM D150 standard of measurements. The provision of springs attached to the electrodes provides the balance

and pressure to establish their proper contact with the loaded dielectric sample for precision measurements. These electrical and dielectric measurements of the films were made at a fixed temperature of 27 °C using both the equipments which covered the broadband frequency range of 20 Hz–1 GHz.

Results and discussion

Physical and morphological properties

The digital pictures of these films are provided in Fig. 1a for having a look at the transparency and surface smoothness, and also the manual test of flexibility and bending. The PMMA film has excellent transparency which is slightly less for the PVDF film, and it seems to a little decrease for the blend films when the amount of PVDF increases. The manual touch realizes the highly smooth surfaces of the films. The bending test infers that these polymer blend films are slightly hard showing their compact packing and reasonable flexibility but not stretchable. Figure 1b depicts the SEM images of pure PVDF film, pure PMMA film, and PVDF/PMMA blend (80/20 wt/wt%) film. The PVDF film has characteristic spherulites of micro-sized separated by fibril-like textures representing its polymorphs, and there are no micro-pores that show its highly compact surface [21]. The SEM image of pristine PMMA film confirms the highly smooth surface which is attributed to the amorphous structure and tight molecular packing because the micro-pores are not noticeable [37]. The SEM image of the PVDF/PMMA blend also

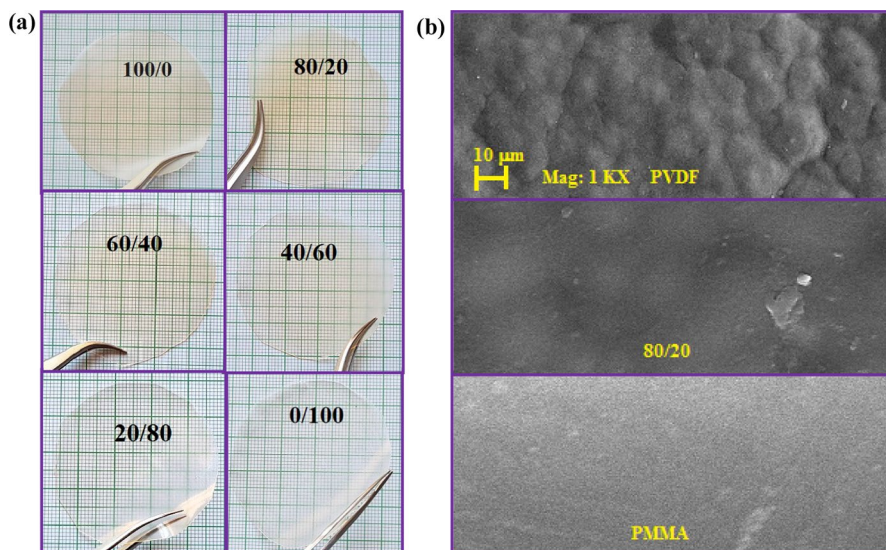


Fig. 1 a Digital photographs of the various compositional ratio PVDF/PMMA blend films (PVDF/PMMA = 100/0, 80/20, 60/40, 40/60, 20/80, and 0/100 wt/wt%) and b SEM images of the pure PVDF film, PVDF/PMMA blend (80/20 wt/wt%) film, and pure PMMA film

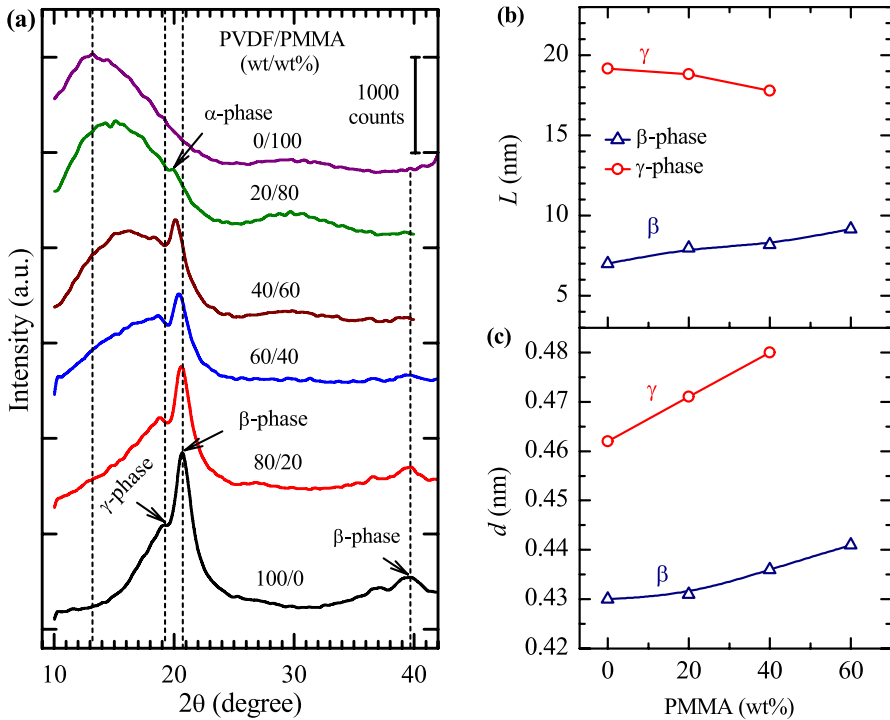


Fig. 2 a XRD patterns of the various compositional ratios PVDF/PMMA blend films (PVDF/PMMA = 100/0, 80/20, 60/40, 40/60, 20/80, and 0/100 wt/wt%) and plots of **b** crystallite size L and **c** interlayer spacing d versus PMMA (wt%) for the various compositional ratios PVDF/PMMA blend films

exhibited spherulite structures of less number but bigger sizes and less imperfect which are surrounded by the smooth regions revealing the formation of a miscible blend with at least the development of some PVDF-rich domains. Additionally, the absence of micro-pores also reveals the formation of a tightly packed surface of the PVDF/PMMA blend film.

XRD traces and structural analysis

To examine the influence of the amorphous PMMA on the polymorphs of semicrystalline PVDF, the diffractograms of the different compositional ratios PVDF/PMMA blend films (PVDF/PMMA = 100/0, 80/20, 60/40, 40/60, 20/80, and 0/100 wt/wt%) are provided one above another in Fig. 2a. The PANalytical X'pert data viewer and analyzer software is used to determine the Bragg angle (2θ), intensity (I), and full width at half maximum (FWHM) of various diffraction peaks that appeared in XRD patterns of the PVDF/PMMA blend films. Additionally, the overlapped diffraction peaks are separated through a deconvolution procedure using OriginLab 8.5 software, and the FWHM values of deconvoluted peaks fairly support that obtained from the X'pert data analyzer software. The

Table 1 Values of Bragg's angle 2θ , crystal reflection plane indices hkl , basal spacing d , full width at half maximum FWHM, crystallite size L , and intensity I of the diffraction peaks of various compositional ratios PVDF/PMMA blend films

PVDF/PMMA films (wt/wt%)	2θ ($^\circ$)	hkl	d (nm)	FWHM ($\times 10^{-3}$ rad)	L (nm)	I (counts)
100/0	19.22 (γ)	(022)	0.462	7.46	19.15	654
	20.67 (β)	(110), (200)	0.430	20.39	6.99	1552
	39.67 (β)	(201), (111)	0.227	32.59	4.18	273
80/20	18.82 (γ)	(022)	0.471	7.60	18.81	573
	20.62 (β)	(110), (200)	0.431	17.84	7.98	1163
	39.72 (β)	(201), (111)	0.227	26.55	5.13	195
60/40	18.62 (γ)	(022)	0.480	8.03	17.79	634
	20.37 (β)	(110), (200)	0.436	17.37	8.20	878
40/60	15.12		0.586	–	–	850
	20.12 (β)	(110)	0.441	15.59	9.15	994
20/80	15.12		0.586	–	–	799
	19.87 (α)	(110)	0.447	3.98	35.83	404
0/100	13.17		0.672	–	–	696

obtained values of these structural parameters along with Miller indices (hkl) corresponding to reflection planes of the assigned crystal phases of the PVDF in these polymer blend films are listed in Table 1. The values of interlayer spacings (d) and crystallite sizes (L) of the various crystals developed in the PVDF/PMMA blend films were evaluated, respectively, by using the Bragg's law Eq. (1) and the Debye–Scherrer relationship Eq. (2) demonstrated previously [21, 38], and these values are listed in Table 1.

$$d = \frac{\lambda}{2 \sin \theta} \quad (1)$$

$$L = \frac{k\lambda}{\beta \cos \theta} \quad (2)$$

where $\lambda = 1.5406 \text{ \AA}$ denotes the wavelength of Cu- K_α X-ray radiation, θ represents the Bragg's angle, k is the crystallites shape factor (also known as Scherrer constant) and its value is most commonly taken as 0.94 for the semicrystalline polymers, and β is the full width at half maximum (FWHM) of the diffraction peaks of PVDF/PMMA blend films. Although the determination of L by the Scherrer equation gives rather a lower bound on the coherently scattering domain size which may or may not be equal to the crystal size. But the study of L gives valuable information, especially about the trends of changes in crystallite shapes with the variation in the amount of the constituents of the composition which we have considered and explained for the PVDF/PMMA blends. Figure 2a illustrates that the XRD pattern of the pristine PVDF film (labelled by 100/0) exhibits different intensities diffraction peaks at 2θ

values of 19.22° , 20.67° , and 39.67° confirming its semicrystalline behaviour which is also supported by the spherulite morphology of this film (Fig. 1b). According to the previous literature [21, 22, 24, 39–43], the shoulder peak appeared at 19.22° can be assigned to the γ -phase of the reflection plane (022). Additionally, the main intense peak and another mild peak were observed, respectively, at 20.67° and 39.67° attributed to the β -crystal phase of reflection planes (110), (200) and (201), (111) revealing its polymorphic character. In the case of PVDF film, the assignments of crystal phases to the exhibited diffraction peaks are still controversial [22]. Here, the main intense peak assigned to β -phase could also have some proportion of α -phase and the same in the case of 19.22° peak. The XRD pattern of pristine PMMA film (labelled as 0/100) exhibited a broad diffraction hump centred around 13.17° confirms the amorphous nature of the PMMA matrix [31, 37] which is also revealed from the highly smooth surface morphology of the solution-cast PMMA film (Fig. 1b).

The XRD patterns of the various compositional ratios PVDF/PMMA blend films (labelled by 80/20, 60/40, 40/60, and 20/80 in Fig. 2a) show that the blending of PMMA with the PVDF modifies the structural characteristics of the γ - and β -crystal phases as evidenced from the shift in their peaks positions which also reflects from an altered morphology of the 80/20 wt/wt% blend film (Fig. 1b). Further, the intensities of these low angle side shifted diffraction peaks gradually decrease with the increase in PMMA amount in the PVDF/PMMA blend which reveals alteration in the amount of dominance phase to that of another merged phase. It can be noted from Fig. 2a that the γ -phase diffraction peak disappeared and a new diffraction peak appeared at $2\theta = 15.12^\circ$ when the compositional ratio was varied and the relative content of amorphous PMMA reaches 40 wt% in the PVDF/PMMA blend. Furthermore, when the content of PMMA raised to 80 wt% in the blend, it seems that the polar β -phase largely reduced and a non-polar α -phase appeared in dominance mode as revealed from the mild peak that was noted at 19.87° belonging to the reflection plane (110) [21, 22]. The decrease in XRD peaks intensities also evidenced that the crystalline content of the PVDF/PMMA blend films decreases with the increasing relative content of amorphous PMMA in the blends that means during film formation, these blends PMMA act as a disturbing factor for the better order of PVDF crystallization.

Figure 2b illustrates the variation in crystallite size L of the β - and γ -crystal phases with the PMMA (wt%) for these PVDF/PMMA blend films. It is noted from this figure that the value of L decreased slightly (from 19.15 to 17.79 nm) for the γ -crystal phase but it increased almost linearly from 6.99 to 9.15 nm for the β -crystal phase (probably the merged α -phase with dominant β -phase) when the amount of PMMA increased in these blend films. This result establishes that the PMMA amount acts as a disturbing factor for the development of smaller sizes dense crystallites of the PVDF and promotes to form of bigger sizes crystallites with lesser density in the PVDF/PMMA blends and simultaneously reduces the size of γ -crystals. This finding also supports the bigger sizes of spherulite morphology that appeared in the PVDF/PMMA blend film. Additionally, from Fig. 2c, one can see that the value of interlayer spacing d increased linearly (from 0.462 to 0.480 nm) for the γ -crystal phase and a little increase for the β -crystal

phase (from 0.430 to 0.441 nm) with increased the content of PMMA in the PVDF/PMMA blend films. This finding suggests the increase in the intercalated amount of the PMMA between the layers of PVDF crystallites and reveals the formation of a miscible blend.

FTIR spectra and confirmation of crystal phases of PVDF

FTIR spectroscopy is a most established versatile technique to identify the occurrence of different bondings and the interactions in the polymer blend and composite materials and the alteration in structures with the variation in blend compositional ratios [16, 21, 38, 44]. Additionally, this technique is frequently used for the identification and assignment of polymorphs in the ferroelectric PVDF polymer matrix [21, 22, 44, 45]. Therefore, the FTIR measurements on PVDF/PMMA blend films are performed to support the XRD results on the structural properties of these blend films. The FTIR transmittance spectra over a wavenumber range of 650–4000 cm^{-1} for the PVDF/PMMA blend films are shown in

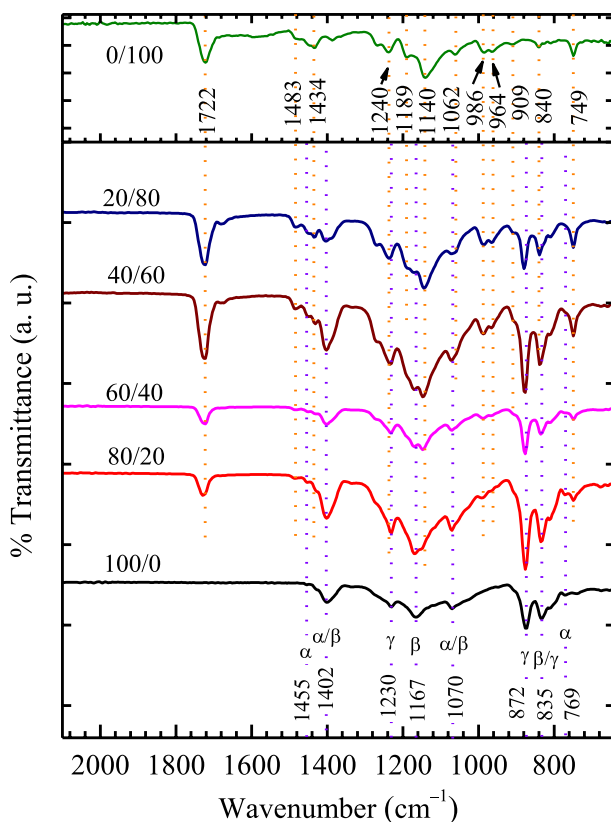


Fig. 3 FTIR transmittance spectra of the various compositional ratios PVDF/PMMA blend films (PVDF/PMMA = 100/0, 80/20, 60/40, 40/60, 20/80, and 0/100 wt/wt%)

Table 2 Wavenumber values of FTIR transmittance bands of different vibrational modes of the groups of the repeat units of PVDF and PMMA chains [assigned as bending δ (δ_s in-plane bending), stretching ν (ν_a symmetric and ν_{as} asymmetric), wagging ω , and rocking ρ (ρ_a symmetric and ρ_{as} asymmetric)] for the PVDF/PMMA blend films of compositional ratios 100/0, 80/20, 60/40, 40/60, 20/80, and 0/100 wt/wt%

Vibrational modes of PVDF	Wavenumber (cm ⁻¹)						Vibrational modes of PMMA
	100/0	80/20	60/40	40/60	20/80	0/100	
	–	749	749	749	749	749	ν C–C/ ω CH ₃
δ_s CF ₂	769(α)	770	772	–	–	–	
ρ CH ₂ , ν CF ₂	835(β/γ)	835	835	839	839	840	ρ CH ₂
	872(γ)	876	877	878	880	–	–
–	–	–	909	909	909	909	ρ O–CH ₃
–	–	966	964	964	964	964	ρ O–CH ₃
–	–	990	986	986	986	986	δ O–CH ₃
–	–	–	–	1062	1062	1062	ν_{as} C–O–C
–	–	1166	1149	1148	1144	1140	ν C–O (doublet)
–	–	–	–	–	1189	1189	
ω CH ₂	1070(α/β)	1070	1070	1070	1070	–	
ν_a CF ₂	1167(β)	1168	1169	1170	1171	–	
ν C–F	1230(γ)	1230	1231	1234	1237	1240	ν_a C–C–O
ν_a CF ₂	1402(α/β)	1402	1402	1402	1405	–	
–	–	1434	1434	1434	1434	1434	ρ_{as} C–CH ₃
δ CH ₂	1455(α)	1452	1451	1149	1147	–	
	–	1483	1483	1483	1483	1483	ρ_{as} C–CH ₂
	–	1729	1725	1726	1724	1722	ν C=O

Fig. 3. The reported FTIR spectra of the studied samples exclude the wavenumber range of 2100–4000 cm⁻¹ because in this range, vibrational modes of PVDF and PMMA are not exhibited. The wavenumbers of various infrared (IR) bands corresponding to structural vibration modes for the PVDF and the PMMA chains are marked by vertical dotted lines in the figure and the same with their assignments are listed in Table 2. The nature of polymer–polymer interactions in these PVDF/PMMA blend materials is explored noting a shift in positions of the various IR bands (i.e. change in bands wavenumbers) and alterations in the bands intensities, and also the shapes as compared to that of the characteristic IR bands of the pristine PVDF and PMMA materials.

The FTIR spectrum of pristine PVDF (denoted by 100/0 in the figure) identifies the presence of polar β - and γ -phases and also non-polar α -phase. Low intensity IR bands exhibited at 769 cm⁻¹ and 1455 cm⁻¹ correspond to the skeletal bending and in-plane bending (scissoring) of the CF₂ and CH₂ functional groups, respectively, which attribute to the PVDF α -phase [21, 42, 46]. An intense IR band appeared at 835 cm⁻¹, representing the stretching and wagging of the CH₂ and CF₂ functional groups, also evidenced by the overlapped β - and γ -phases [21, 22, 44, 45]. The bands displayed at 872 cm⁻¹ and 1230 cm⁻¹ correspond

to stretching of the CF_2 and C–F functional groups, respectively, which can be assigned to the γ -phase of PVDF [22, 44, 45]. Furthermore, the other intense or weak IR bands displayed at 1070, 1167, and 1402 cm^{-1} can be assigned to the wagging and symmetric stretching of the CH_2 and CF_2 functional groups of the PVDF repeat unit, respectively. The IR bands appeared at 1070 cm^{-1} and 1402 cm^{-1} can be assigned to the overlapped α - and β -phases, while another band at 1167 cm^{-1} can be attributed to the β -phase [22, 44, 45]. According to a comparative survey of the literature, FTIR results may cause some confusion in the assignment of the α -, β - and γ -crystal phases, and therefore, their comparison is a must with the phases identified by XRD and DSC results [22] which we have performed in this study. The FTIR spectrum of PMMA is shown in the upper layer of Fig. 3. This spectrum displayed the intense or weak bands at 749, 840, 909 and 964, 986, 1062, 1140 and 1189, 1240, 1434, 1483, and 1722 cm^{-1} corresponding to the C–C stretching/ CH_3 wagging, CH_2 rocking, O– CH_3 rocking, O– CH_3 in-phase bending, C–O–C asymmetric stretching, C–O stretching, C–C–O symmetric stretching, C– CH_3 asymmetric bending, C– CH_2 asymmetric bending, and C=O stretching vibration of carbonyl groups, respectively, as demonstrated in earlier literature [47, 48].

Figure 3 shows that the characteristic vibrational modes of PVDF which belongs to its various crystals phase are significantly altered due to the addition of PMMA and that these vibrational modes showed further change as the PVDF/PMMA blend compositional ratio is varied. It is observed that the IR bands of the PVDF in the PVDF/PMMA blends relatively shifted to higher wavenumbers in comparison with the pristine PVDF bands with some uneven variations in their intensities indicating some alteration in the amount of crystal phases. Also, some new IR bands appeared in the FTIR spectra of the blends which are consistent with PMMA. The bands of PVDF in the 80/20 wt/wt% PVDF/PMMA blend are slightly altered. But increasing the PMMA concentration to 80 wt% in the blend considerable changes in the positions of the IR bands of PVDF and PMMA could be observed, and some new IR bands of PMMA appeared at 909, 1062, and 1189 cm^{-1} . The weak IR band of PVDF at 769 cm^{-1} disappeared when the PMMA concentration increased to 60 wt% in the blend films. However, the intensity of the IR band at 1455 cm^{-1} slightly increases with increased concentration of PMMA, which suggested the presence of α -phase in all PVDF/PMMA blend films. The co-existence of most of the PVDF and PMMA of the characteristic IR bands in the FTIR spectra of PVDF/PMMA blends evidence the formation of a miscible blend that is owing to hydrogen bond interactions between the functional groups of these polymers [46]. In the PVDF/PMMA blend films, the IR bands for pristine PMMA at 1140 cm^{-1} and 1722 cm^{-1} correspond to stretching vibration of C–O and C=O polar functional groups and are shifted to the higher wavenumber side in all the PVDF/PMMA blend compositions. This shift is caused by the interaction between the ester and carbonyl groups of the PMMA with the CH_2 groups of the PVDF chain, which also indicates the formation of compatible blends of these two constituents [45, 47].

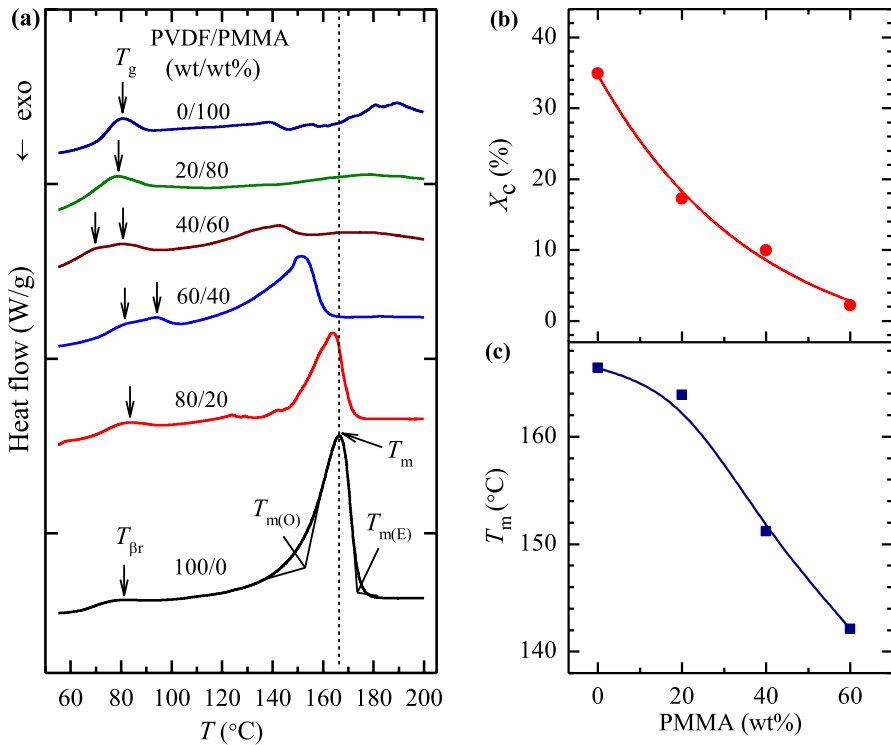


Fig. 4 a DSC thermograms of various compositional ratios PVDF/PMMA blend films (PVDF/PMMA = 100/0, 80/20, 60/40, 40/60, 20/80, and 0/100 wt/wt%), and plots of **b** X_c (%) and **c** T_m (°C) versus PMMA (wt%) for the PVDF/PMMA blend films. Solid lines represent **b** exponential fit of data and **c** B-spline fit of data points

DSC thermograms

Thermal transition and degree of crystallinity of the PVDF crystallites in the different compositional ratios PVDF/PMMA blend films were explained from analysis of their DSC thermograms of temperature range from 55 to 200 °C (Fig. 4a). The thermogram of pristine PVDF film exhibited two endothermic peaks. A weak endothermic peak observed at 81.3 °C can be assigned to the β -phase recrystallization temperature $T_{\beta r}$ as explained in the literature [49] because its glass transition is exhibited at about -40 °C [50]. The intense complex endothermic peak at 166.4 °C belongs to a melting temperature T_m of the dominant β -phase crystal of the PVDF [13, 22–24, 32, 42] but its asymmetric distribution indicates the involvements of α -phase also. This finding from the DSC trace also favours the XRD results on the existence of both the phases (a small amount of α -phase merged with dominant β -phase) in the pristine PVDF film which was also revealed from the FTIR results and morphological analysis. The pristine PMMA film exhibited a narrow peak at 80.6 °C which is attributed to its glass transition temperature T_g [51]. The pristine

PMMA structure is less flexible thus leading it relatively high value of glass transition temperature [52].

It can be noted from Fig. 4a that the glass transition temperature peak related to PMMA in the PVDF/PMMA blend films largely changes in shape and intensity when the blend composition ratio varied from 20/80 to 80/20 wt/wt% in the step of 20. For the PMMA-rich blend having 20/80 wt/wt% composition, the T_g of PMMA appeared, but the blends 40/60 and 60/40 wt/wt% have this broader peak with the signature of overlapping the PMMA glass transition peak with the β -phase recrystallization peak of PVDF (marked with the vertical down arrow in the figure). The fact that we don't see it at 80/20 wt/wt% blend might be because it is simply too weak and masked by the PVDF β -phase recrystallization phenomenon. The T_g values of PMMA and $T_{\beta r}$ of PVDF noted from the DSC traces of these PVDF/PMMA blend films are listed in Table 3.

The degree of crystallinity X_c (%) of PVDF/PMMA blend films which represents the amount of PVDF crystallites in the blend can be determined by the melting enthalpy-based relationship given in Eq. (3) [24, 31]:

$$X_c(\%) = \left(\frac{\Delta H_m}{\Delta H_m^*} \right) \times 100 \quad (3)$$

The ΔH_m values of the PVDF/PMMA blend films are taken equal to the area under the endothermic peak in the DSC traces and ΔH_m^* is the melting enthalpy for a 100% crystalline PVDF [104.5 (J g⁻¹)] [24]. The onset melting temperature $T_{m(O)}$, peak melting temperature T_m or $T_{m(P)}$, end melting temperature $T_{m(E)}$, melting temperature range $\Delta T_m = T_{m(E)} - T_{m(O)}$, melting enthalpy ΔH_m , and the degree of crystallinity X_c (%) of the PVDF crystallites in these PVDF/PMMA blend films were obtained from DSC traces and listed in Table 3.

It is explored that when a relative amount of PMMA increases (≥ 40 wt%) in the PVDF/PMMA blend films, the value of $T_{m(O)}$ decreases at a greater rate than the $T_{m(E)}$ (Table 3). Thus, the value of ΔT_m increases and consequently the range of the melting process of the PVDF crystallites expands largely. These results are

Table 3 Values of β -phase recrystallization temperature of PVDF $T_{\beta r}$, glass transition temperature of PMMA T_g , PVDF crystals onset melting temperature $T_{m(O)}$, peak melting temperature T_m , end melting temperature $T_{m(E)}$, melting temperature range ΔT_m , and melting enthalpy ΔH_m , and the degree of crystallinity X_c with respect to the PVDF component determined from the DSC endothermic peaks of various compositional ratios PVDF/PMMA blend films

PVDF/PMMA films (wt/wt%)	$T_{\beta r}$, T_g (°C)	$T_{m(O)}$ (°C)	T_m (°C)	$T_{m(E)}$ (°C)	ΔT_m (°C)	ΔH_m (J/g)	X_c (%)
100/0	81.3	152.7	166.4	173.6	20.9	36.48	34.9
80/20	83.5	150.8	163.9	170.5	19.7	18.07	17.3
60/40	81.6, 94.1	137.7	151.2	160.2	22.5	10.42	10.0
40/60	69.2, 80.7	123.5	142.1	149.6	26.1	2.29	2.2
20/80	79.0	–	–	–	–	–	–
0/100	80.6	–	–	–	–	–	–

obtained due to the formation of more imperfect PVDF crystals with the increased amount of PMMA in the formulated blend compositions as argued earlier [24, 53]. The obtained X_c (%) values are plotted in Fig. 4b which confirmed that the degree of crystallinity of the PVDF decreases exponentially with the increase in PMMA amount in the blend films. The pristine PVDF crystallinity is 34.9% and it drops to 2.2% when the PVDF/PMMA blend was prepared with a 40/60 wt/wt% compositional ratio. The XRD pattern of PVDF/PMMA (labelled by 20/80) blend film has a little peak showing its almost amorphous character, and this fact is also favoured by its DSC thermogram. Such a large decrease in the degree of crystallinity of these blend films with the increase in PMMA amount (especially for PMMA-rich blends) is simply the fact that PMMA chains disturb the order formation of PVDF chains structures.

Figure 4c shows that the melting temperature T_m of PVDF crystallites also decreases when the amount of PMMA increases in the PVDF/PMMA blend films. A drop of about 24 °C is found in the T_m value for 40/60 wt/wt% compositional ratio PVDF/PMMA blend film in comparison with that of the pristine PVDF film (Table 3). This decrease in the melting temperature is associated with a decrease in the chemical potential of PVDF when it is blended with amorphous PMMA [31]. From this result and also detailed discussion on the glass transition temperature, melting temperature, and degree of crystallinity of the PVDF/PMMA blend films over the entire compositional ratio, we also suggest a miscible blend formation of the blended semicrystalline PVDF and amorphous PMMA which favours the earlier findings [24, 31, 49, 54–57]. The results of this work and the previous studies on these blends evidenced that the PVDF and PMMA miscibility arises due to the intermolecular chain interactions which are either through the oxygen atoms of the carbonyl groups of PMMA and the hydrogen atoms of PVDF or the dipole–dipole interaction between the CH_2 groups of the PMMA chain and the CF_2 groups of the PVDF chain [32, 58]. Besides this interpretation and reported facts about the formation of miscible PVDF/PMMA blend, the presented structural results on the PVDF crystallites also evidenced that there is always the possibility of the formation of a quite pure PVDF phase in all these different composition blends.

Dielectric dispersion and relaxation processes

Dielectric dispersion behaviour of a dielectric material as a function of harmonic electric field frequency is concerned with the electric energy storage ability and the dielectric loss (energy dissipation) by the material at a fixed temperature [1, 3, 7, 11, 15, 21, 38], and it is defined by complex dielectric permittivity function ϵ^* given in Eq. (4) [3, 20]:

$$\epsilon^* = \epsilon' - j\epsilon'' \quad (4)$$

where the real part ϵ' refers to dielectric permittivity which is a measure of the energy storage capacity of a dielectric material and the imaginary part ϵ'' is the dielectric loss which identifies the amount of stored electromagnetic energy converted into the heat per cycle by Joule heating effect. This loss part is related to different

physical processes that occurred in the dielectric like electrical conduction, dielectric relaxation, dielectric resonance, etc., whereas the energy storage part represents the magnitude of dielectric polarization processes which are mostly the applied harmonic electric field frequency-dependent. For identification of the suitability of dielectric material in the development of energy storage devices, it must have an appreciably high value of ϵ' and a reasonably low value of ϵ'' [1, 4, 5]. Furthermore, the ϵ' values must remain stable over a broader frequency window to work the device satisfactorily under the influence of different frequency harmonic fields [4, 8, 11, 12]. The ϵ' values for the PVDF/PMMA blend films were determined by the capacitive measurement method using the relation given in Eq. (5) [4, 59]:

$$\epsilon' = \frac{t_g C_p}{\epsilon_0 A} \tag{5}$$

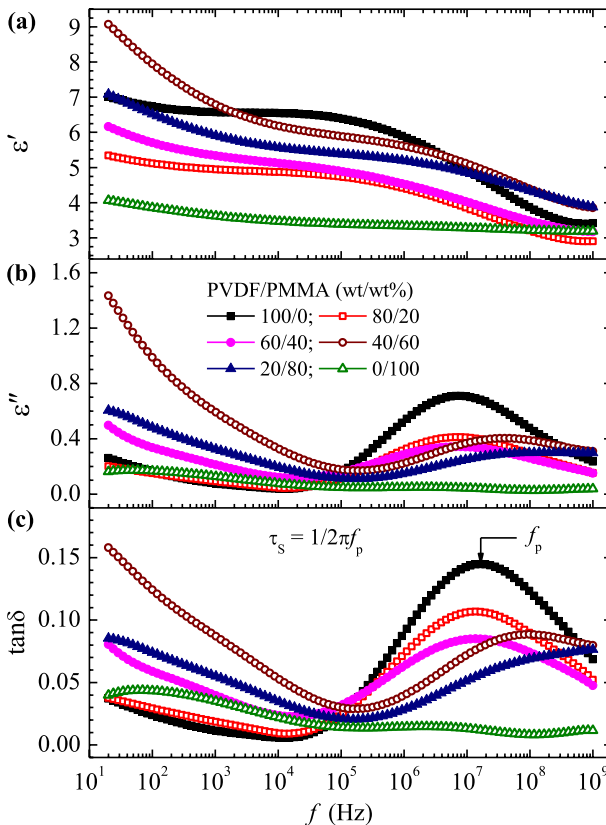


Fig. 5 Broadband frequency range (20 Hz to 1 GHz) complex dielectric permittivity spectra (**a** real part ϵ' and **b** imaginary part ϵ'') and **c** dielectric loss tangent ($\tan\delta$) for the various compositional ratios PVDF/PMMA blend films (PVDF/PMMA = 100/0, 80/20, 60/40, 40/60, 20/80, and 0/100 wt/wt%) at 27 °C

where t_g is the film thickness, A is the surface area of the active electrode of the test fixture, C_p is the capacitance of the test fixture loaded with the dielectric sample, and $\epsilon_0 = 8.854 \times 10^{-12} \text{ F m}^{-1}$ is the dielectric permittivity in a vacuum. The ϵ'' values for these films were determined from their frequency-dependent ϵ' and $\tan\delta$ values using the following relationship given in Eq. (6) [3, 15, 38, 59]:

$$\epsilon'' = \epsilon' \tan \delta \quad (6)$$

Figure 5 shows the ϵ' , ϵ'' , and $\tan\delta$ spectra of the PVDF/PMMA blend films covering a broader frequency range from 20 Hz to 1 GHz of the applied harmonic electric field at a fixed temperature of 27 °C. One can understand from this figure that the values of all these dielectric functions change with the variation in frequency and also the polymers compositional ratio in the PVDF/PMMA blends. These blends exhibited a decrease in ϵ' values in various characteristic steps when the frequency increases, and finally attained the study state. Furthermore, the ϵ' values of these blend films change anomalously in the range of about 4–9, at 20 Hz, with the variation in blend compositional ratio which leads to their appropriateness as dielectric materials in power frequency devices, whereas observed values in the range of about 2.8–3.8 at 1 GHz confirm their suitability as a flexible dielectric substrate for the development of microwave devices. The structural parameters established that there is significant variation in the polar β -phase and also the signature of α -phase merged with β -phase which changes irregularly with the variation in constituents composition of these polymer blends which causes anomalous variation in their ϵ' values at a fixed frequency. This behaviour of ϵ' values with structural changes establishes a structure-property relationship for the varying composition PVDF/PMMA blend materials. According to previous literature on dielectric materials [1, 4, 6, 7, 9, 13, 39, 60, 61], dispersion behaviour of ϵ' values reveals that among these polymer blends of high ϵ' and low ϵ'' could be potential candidates for the development of energy storage devices. Additionally, low ϵ' blends can be used as dielectric substrates in high-frequency OFETs, integrated microelectronic devices, and flexible-type microwave devices. The high-loss blend materials (high ϵ'' in the relaxation frequency range) also suggest their appropriateness for electromagnetic interference (EMI) shielders.

Several characteristic features of dielectric dispersion related to broadband frequency range ϵ' spectra of the PVDF/PMMA blend films can be noted in Fig. 5a. The decrease in ϵ' values at a lower range of frequencies is associated with the Maxwell–Wagner–Sillars (MWS) type interfacial polarization (IP) process which in general exhibited in the semicrystalline polymers, polymer blends, and the polymer matrices-based composites having different conductivity constituents as defined in detail in the literature [14, 15, 26, 39, 62, 63]. The magnitude of the IP process (MWS) is strongly ruled by the type of dielectric material which means its formation is mild for non-polar dielectrics which enhances when some charge carriers are available in the dielectric to displace some short distances and it appears very strong in the dielectric having ion-dipole complexes. The interfacial polarization in the PVDF and PVDF/PMMA blends is caused due to the accumulation of displaced charges at the interfaces of the crystalline and amorphous domains or the domains

of different types of crystallites in these polymeric dielectric materials [15, 38, 39, 62].

A small dispersion of ϵ' values at low experimental frequencies for the PVDF and its blends with PMMA infers that the contribution of the MWS process in these dielectrics is small. The variation in ϵ' values of the PMMA film is noted relatively low (from 4.1 to 3.2) with a wide range of frequency variation (over a nine orders of magnitude) confirming it as a low-dielectric material of almost frequency independent polarization performance [37, 50]. This dielectric dispersion behaviour makes the pristine PMMA film the most appropriate dielectric material for applications as a gate insulator in organic thin-film transistors (OTFTs) and low-dielectric material as a substrate in the fabrication of microelectronic devices [33, 34, 37, 50, 60]. The relatively high ϵ' values of the PVDF film in comparison with that of the PMMA film are owing to the formation of the polar β -phase of the PVDF which was thoroughly discussed in the previous sections “XRD traces and structural analysis–DSC thermograms”. The appreciable decrease in ϵ' values of the PVDF and PVDF/PMMA blend films with an increasing frequency above 1 MHz is attributed to molecular polarization that explains the existence of the chain segmental relaxation process (α -relaxation) of the PVDF as demonstrated in the literature [8, 12, 13, 61, 64]. The dielectric studies on a variety of polymers and nanocomposites also demonstrated the dielectric dispersion and occurrence of structural relaxations in such materials in the 1 MHz–1 GHz range [7, 10, 11, 65, 66]. For the benefit of readers and also to the technocrats and industrial users, the ϵ' values of all the PVDF/PMMA blends at 100 Hz, 10 kHz, 1 MHz, 100 MHz, and 1 GHz are provided in Table 4, which may also be interesting for dielectric modelling of these polymer blend materials.

The ϵ'' and $\tan\delta$ spectra shown in Fig. 5b, c reveal that the PVDF/PMMA blend films have the chain segmental relaxation process (α -relaxation) in the higher experimental frequency region. The characteristic features of this peak that appeared in the PVDF/PMMA blend seem identical to that of the PVDF film which suggests that in the miscible blend, some PVDF-rich PVDF/PMMA domains exist and the dynamics of the PVDF α -relaxation process in these domains is largely influenced by the existed small PMMA amount in the domains. The assumption of PVDF-rich

Table 4 Values of dielectric permittivity ϵ' and dielectric loss tangent $\tan\delta$ (ϵ''/ϵ') at fixed frequencies f of 100 Hz, 10 kHz, 1 MHz, 100 MHz, and 1 GHz for the various compositional ratios PVDF/PMMA blend films at 27 °C

PVDF/ PMMA films (wt/wt%)	$f=100$ Hz		$f=10$ kHz		$f=1$ MHz		$f=100$ MHz		$f=1$ GHz	
	ϵ'	$\tan\delta$	ϵ'	$\tan\delta$	ϵ'	$\tan\delta$	ϵ'	$\tan\delta$	ϵ'	$\tan\delta$
100/0	6.75	0.023	6.56	0.005	5.87	0.090	3.84	0.122	3.15	0.069
80/20	5.10	0.029	4.87	0.009	4.40	0.072	3.20	0.089	2.90	0.052
60/40	5.69	0.058	5.11	0.023	4.53	0.063	3.46	0.074	3.17	0.047
40/60	7.93	0.125	6.19	0.052	5.60	0.040	4.39	0.088	3.86	0.080
20/80	6.50	0.073	5.56	0.034	5.19	0.030	4.34	0.069	3.88	0.076
0/100	3.86	0.044	3.46	0.022	3.33	0.014	3.21	0.008	3.19	0.017

dynamical domains in the miscible PVDF/PMMA blend is with the consideration of its SEM image given in Fig. 1b. The pristine PVDF film exhibited a highly intense α -relaxation peak around 15 MHz, and its intensity is reduced significantly for the PVDF/PMMA blend films which further shows some variation in intensity and the position on the frequency scale with the variation in polymer blend compositional ratio. The position of this relaxation peak on the frequency scale anomalously changes with the variation in constituents composition in these PVDF/PMMA blend films revealing that the hindrance to this process alters in presence of PMMA and also changes with its blended amount. In comparison with the PVDF and PVDF/PMMA blend films, the pristine PMMA film displayed two relaxation peaks of very low intensities around 100 Hz and 5 MHz which can be assigned to its high rigid chain segmental motion (α -relaxation) and the dipolar rotational motion (β -relaxation), respectively [37, 50, 60, 67]. The β -relaxation peak is obtained due to the rotation of the ester functional group ($-\text{COOCH}_3$) around the C–C bond of the repeat unit that connects it to the main PMMA chain [60, 67]. The values of the relaxation time τ_s (also denoted by τ_α) for the PVDF, PMMA, and the PVDF/PMMA blend films and the τ_D (τ_β) for pure PMMA film were determined using Eq. (7) [21]:

$$\tau_s = \frac{1}{2\pi f_p} \tag{7}$$

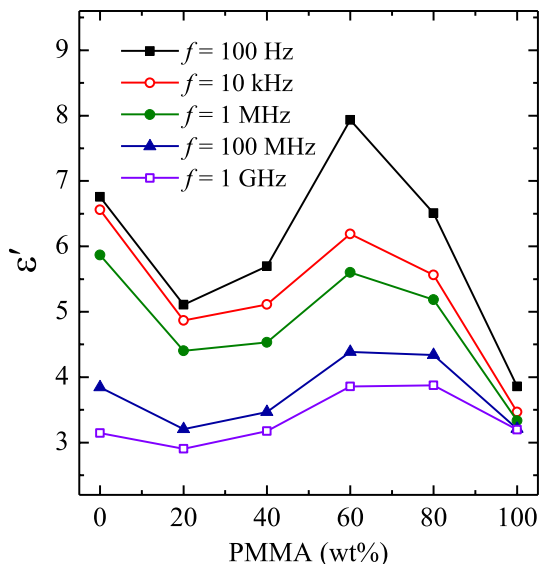
where f_p is the frequency value of the peak that appeared in $\tan\delta$ spectrum representing the relaxation process and it is marked for the PVDF film as a representative sample in Fig. 5c. The calculated values of τ_s of these PVDF/PMMA blend films are listed in Table 5. The variation in the τ_s values confirms a huge alteration in the segmental motion of the PVDF chains with the variation in blended PMMA amount for various compositional ratios of the PVDF/PMMA blend materials.

Figure 6 explains the variation in ϵ' values of the PVDF/PMMA blend films with PMMA (wt%) amount at fixed frequencies of 100 Hz, 10 kHz, 1 MHz, 100 MHz, and 1 GHz and temperature of 27 °C. The obtained plots confirm that the trend in change of ϵ' values of different compositional ratios PVDF/PMMA blend films at all these fixed frequencies is almost identical. This figure also identifies that the ϵ' values change anomalously with the relatively increased amount of PMMA in the blend films. An initial blending of 20 wt% PMMA reduced the ϵ' values, but enhances again with an increase in PMMA amount and exhibited the maximum ϵ' values for

Table 5 Values of PVDF chain segmental motion relaxation time τ_s (also denoted by τ_α) and PMMA dipolar rotational motion relaxation time τ_D (also denoted by τ_β) for the various compositional ratios PVDF/PMMA blend films at 27 °C

PVDF/PMMA films (wt/wt%)	τ_s (s)	τ_D (s)
100/0	9.1×10^{-9}	–
80/20	11.7×10^{-9}	–
60/40	9.9×10^{-9}	–
40/60	1.8×10^{-9}	–
20/80	–	–
0/100	1.8×10^{-3}	48.2×10^{-9}

Fig. 6 Plots of ϵ' versus PMMA (wt%) at fixed frequencies ($f=100$ Hz, 10 kHz, 1 MHz, 100 MHz, and 1 GHz) for the various compositional ratios PVDF/PMMA blend films at 27 °C



the PVDF/PMMA blend of 40/60 (wt/wt%). After this concentration, the ϵ' values decrease for the PVDF/PMMA film of 20/80 (wt/wt%) and then for pristine PMMA film. These results evidence that the ϵ' values can be tailored with the frequency variation as well as the polymer compositional ratio of the PVDF/PMMA blends. It is further revealed that the PVDF/PMMA blend exhibited maximum ϵ' values at all the frequencies when its degree of crystallinity turned close to zero. This finding explains that the PVDF in an amorphous state has better polarizability in the formulated PVDF/PMMA blends.

AC electrical conductivity

The frequency-dependent AC electrical conductivity (real part σ') of dielectric material is associated with its dielectric loss ϵ'' as defined in Eq. (8) [11, 14, 38, 39]:

$$\sigma' = \omega \epsilon_0 \epsilon'' \quad (8)$$

Figure 7 illustrates the dispersion behaviour of σ' with frequency variation from 20 Hz to 1 GHz for the PVDF, PMMA, and their blends. On the log–log scale, σ' values of these polymer blend films increase linearly with the increase in frequency in the lower experimental frequency region and then turned slightly nonlinear from the onset frequency range of the α -relaxation process. It may be noted that the σ' values are very low ($< 10^{-11}$ S cm $^{-1}$) for the PVDF/PMMA blend materials at 20 Hz confirming their high insulation behaviour. The MWS-type interfacial polarization is responsible for the low value of σ' at the lower

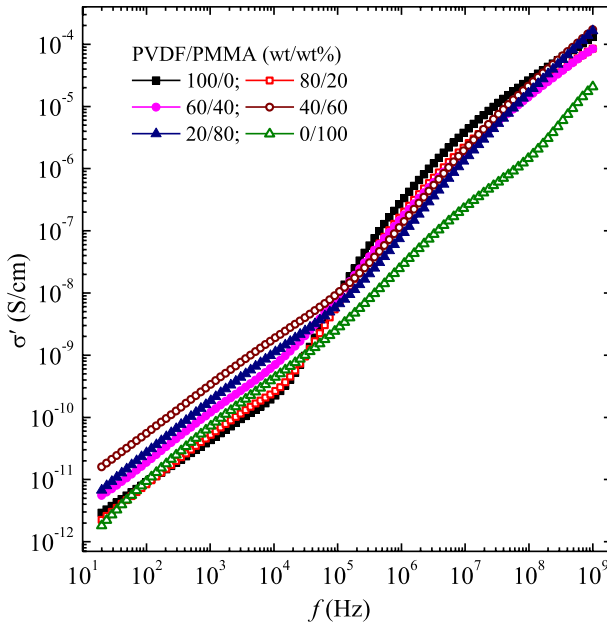


Fig. 7 Broadband frequency range (20 Hz–1 GHz) AC electrical conductivity spectra (real part σ') for various compositional ratios PVDF/PMMA blend films (PVDF/PMMA = 100/0, 80/20, 60/40, 40/60, 20/80, and 0/100 wt/wt%) at 27 °C

frequency region in such types of polymer dielectric materials [68, 69]. The interfaces between the segments and/or domains of the PVDF and PMMA in their blends behave like potential barriers for the charge carriers at the lower frequencies reducing the probability of the carriers overcoming these potential barriers, and hence, the conduction is poor. However, in the high-frequency region, the charge carriers have enough energy to overcome such types of potential barriers, and hence, the value of σ' increases. The σ' values also exhibited anomalous behaviour, at a fixed frequency, when the PMMA content increased in the PVDF/PMMA blend films.

Conclusions

This paper reported the morphology, crystalline phases of the PVDF and their degree of crystallinity and melting temperatures, along with the broadband frequency range (20 Hz–1 GHz) dielectric and electrical dispersion behaviour of the different compositional ratios PVDF/PMMA blend films. The XRD and FTIR results confirm the distinguishable or co-existence of α -, β - and/or γ -crystal phases of the PVDF and their amounts largely change with the variation in PVDF/PMMA blend compositional ratio. The SEM images explain the spherulite morphology of the PVDF and the highly smooth surface of PMMA with the tight molecular packing which also appeared in their blends. It is explored that the

initial addition of 20 (wt%) PMMA amount with the 80 (wt%) PVDF, and then further increase in PMMA amount over the entire compositional ratio enhanced the PVDF amorphous phase and turned the PVDF/PMMA blend of 40/60 wt/wt% almost amorphous. DSC thermograms demonstrated that the melting temperature T_m , melting enthalpy ΔH_m , and degree of crystallinity X_c (%) of the PVDF crystallites decreased due to the initial addition of PMMA and then further increase in its concentration in the PVDF/PMMA blends. A comparative analysis of XRD, FTIR, and SEM results explains that the PVDF/PMMA blends are miscible over the entire compositional ratio but there is also the existence of PVDF-rich domains. The morphological, structural, and controllable thermal properties demonstrate that these flexible polymeric blend materials may be promising host matrices for the development of advanced polymeric nanocomposites.

The analysis of broadband dielectric dispersion confirmed that the ϵ' values of these PVDF/PMMA blend films at 20 Hz can be achieved in the range of 4–9 with the adjustment of polymer compositional ratios whereas from 2.8 to 3.8 at 1 GHz when they are used at 27 °C. Furthermore, the interfacial polarization has some contribution to the dielectric permittivity at lower frequencies, whereas the dipolar polarization largely ruled the permittivity values at higher radio frequencies. The chain segmental relaxation process is identified in the radio frequency range for the PVDF and PVDF/PMMA blends, and this relaxation is largely influenced by the PMMA amount in the PVDF-rich domains of the blends. All these blends have low electrical conductivity suggesting their suitability for electrical insulators in the design and development of wider frequency AC field operative microelectronic devices. These polymeric blend materials of characteristic structural, thermal, dielectric, and electrical properties could be potential candidates for use as dielectric substrates and insulators in the manufacturing of a variety of flexible-type microelectronic devices, energy storage tunable capacitors workable up to microwave frequencies, flexible-type high radio frequency antenna, and EMI shielders.

Acknowledgements The University Grants Commission, New Delhi, is gratefully acknowledged for the experimental grant through SAP DRS-II Project Grant [No. F.530/12/DRS-II/2016(SAP-I)].

Declarations

Conflict of interest The authors declare that they have no conflict of interest.

References

1. Tan DQ (2020) The search for enhanced dielectric strength of polymer-based dielectric: a focused review on polymer nanocomposites. *J Appl Polym Sci* 137:49379
2. Rajeevan S, John S, George SC (2021) Polyvinylidene fluoride: a multifunctional polymer in supercapacitor applications. *J Power Sour* 504:230037
3. Prateek TVK, Gupta RK (2016) Recent progress on ferroelectric polymer-based nanocomposites for high energy density capacitors; synthesis, dielectric properties, and future aspects. *Chem Rev* 116:4260–4317
4. Zha JW, Zheng MS, Fan BH, Dang ZM (2021) Polymer-based dielectrics with high permittivity for electric energy storage: a review. *Nano Energy* 89:106438

5. Behera R, Elanseralathan K (2022) A review on polyvinylidene fluoride polymer based nanocomposites for energy storage applications. *J Energy Storage* 48:103788
6. Olariu MA, Hamciuc C, Neacsu OM, Hamciuc E, Dimitrov L (2019) Microwave dielectric properties of polyimide composites based on TiO₂ nanotubes and carbon nanotubes. *Dig J Nanomater Biostruct* 14:37–44
7. Singha S, Thomas MJ (2008) Permittivity and tan delta characteristic of epoxy nanocomposites in the frequency range of 1 MHz–1 GHz. *IEEE Trans Dielectr Electr Insul* 15:2–11
8. Zhou W, Li T, Yuan M, Li B, Zhong S, Li Z, Liu X, Zhou J, Wang Y, Cai H, Dang ZM (2021) Decoupling of inter-particle polarization and intra-particle polarization in core–shell structured nanocomposites towards improved dielectric performance. *Energy Storage Mater* 42:1–11
9. Jeon H, Jin S, Shin KY (2022) Highly flexible, high-performance radio-frequency antenna based on free-standing graphene/polymer nanocomposite film. *Appl Surf Sci* 582:152455
10. Sengwa RJ, Dhatarwal P (2021) PVA/MMT and (PVA/PVP)/MMT hybrid nanocomposites for broad-range radio frequency tunable nanodielectric applications. *Mater Lett* 299:130081
11. Sengwa RJ, Dhatarwal P (2022) Toward multifunctionality of PEO/PMMA/MMT hybrid polymer nanocomposites: promising morphological, nanostructural, thermal, broadband dielectric, and optical properties. *J Phys Chem Solids* 166:110708
12. Sengwa RJ, Dhatarwal P (2022) Crystalline phases thermal behaviour and radio frequencies dielectric properties of PVDF/PEO/metal oxides hybrid polymer nanocomposites films. *J Polym Res* 29:186
13. Dhatarwal P, Sengwa RJ (2022) Crystalline phases thermal behaviour, optical energy band gap, and broadband radio wave frequency dielectric properties of PEO/PVDF blend films. *Macromol Res* 30:460–469
14. Chen S, Chen S, Qiao R, Xu H, Liu Z, Luo H, Zhang D (2021) Enhanced dielectric constant of PVDF-based nanocomposites with one dimensional core-shell polypyrrole/sepilolite nanofibers. *Compos A Appl Sci Manuf* 145:106384
15. Sengwa RJ, Dhatarwal P (2021) Nanofiller concentration-dependent appreciably tailorable and multifunctional properties of (PVP/PVA)/SnO₂ nanocomposites for advanced flexible device technologies. *J Mater Sci Mater Electron* 32:9661–9674
16. Dhatarwal P, Sengwa RJ (2019) Impact of PVDF/PEO blend composition on the β -phase crystallization and dielectric properties of silica nanoparticles incorporated polymer nanocomposites. *J Polym Res* 26:196
17. Brunengo E, Conzatti L, Schizzi I, Buscaglia MT, Canu G, Curecheriu L, Costa C, Castellano M, Mitoseriu L, Stagnaro P, Buscaglia V (2021) Improved dielectric properties of poly(vinylidene fluoride)–BaTiO₃ composites by solvent-free processing. *J Appl Polym Sci* 138:50049
18. El-Sayed S, Farag ZR, Saber S (2020) Dielectric relaxations and optical properties of polyvinylidene fluoride/chitosan films. *AIP Adv* 10:095127
19. Kumar N, Sengwa RJ, Dhatarwal P, Saraswat M (2022) Effectively polymer composition controllable optical properties of PVDF/PMMA blend films for advances in flexible devices technologies. *Indian J Eng Mater Sci* 29:169–180
20. Tsonos C, Zois H, Kanapitsas A, Soin N, Siores E, Peppas GD, Pyrgioti EC, Sanida A, Stavropoulos SG, Psarras GC (2019) Polyvinylidene fluoride/magnetic nanocomposites: dielectric and thermal response. *J Phys Chem Solids* 129:378–386
21. Dhatarwal P, Sengwa RJ (2019) Polymer compositional ratio-dependent morphology, crystallinity, dielectric dispersion, structural dynamics, and electrical conductivity of PVDF/PEO blend films. *Macromol Res* 27:1009–1023
22. Martins P, Lopes AC, Lanceros-Mendez S (2014) Electroactive phases of poly(vinylidene fluoride): determination, processing and applications. *Prog Polym Sci* 39:683–706
23. Chiu FC, Chen CC, Chen YJ (2014) Binary and ternary nanocomposites based on PVDF, PMMA, and PVDF/PMMA blends: polymorphism, thermal, and rheological properties. *J Polym Res* 21:378
24. Zhao X, Chen S, Zhang J, Zhang W, Wang X (2011) Crystallization of PVDF in the PVDF/PMMA blends precipitated from their non-solvents: special “orientation” behavior, morphology, and thermal properties. *J Cryst Growth* 328:74–80
25. Qiu J, Gu Q, Sha Y, Huang Y, Zhang M, Luo Z (2022) Preparation and application of dielectric polymers with high permittivity and low energy loss: a mini review. *J Appl Polym Sci* 139:52367
26. Liu Y, Gao J, Yao R, Zhang Y, Zhao T, Tang C, Zhong L (2020) Enhanced energy storage performance in a PVDF/PMMA/TiO₂ blending nanodielectric material. *Mater Chem Phys* 250:123155

27. Mishra J, Tiwari SK, Abolhasani MM, Azimi S, Nayak GC (2017) Fundamental of polymer blends and its thermodynamics. In: Thomas S, Mishra R, Kalarikkal N (eds) Micro and nano fibrillar composites (MFCs and NFCs) from polymer blends. Woodhead Publishing, Sawston, pp 27–55
28. Shi Z, Ma X, Zhao G, Wang G, Zhang L, Li B (2020) Fabrication of high porosity nanocellular polymer foams based on PMMA/PVDF blends. *Mater Des* 195:109002
29. Abolhasani MM, Arani AJ, Nazockdast H, Guo Q (2013) Poly(vinylidene fluoride)-acrylic rubber partially miscible blends: crystallization within conjugated phases induce dual lamellar crystalline structure. *Polymer* 54:4686–4701
30. Weng Z, Wu M, Ren Q, Li W, Zhu X, Wang L, Li H, Zheng W (2022) Achieving low-thermal conductivity and high β phase in PVDF/PMMA blend foams via low-pressure microcellular foaming. *J Appl Polym Sci* 139:52338
31. Aid S, Eddhahak A, Khelladi S, Ortega Z, Chaabani S, Tcharkhtchi A (2019) On the miscibility of PVDF/PMMA polymer blends: thermodynamics, experimental and numerical investigations. *Polym Test* 73:222–231
32. Yang JH, Zhang YS, Xue F, Liu DF, Zhang N, Huang T, Wang Y (2021) Structural relaxation and dielectric response of PVDF/PMMA blend in the presence of graphene oxide. *Polymer* 229:123998
33. Mohammed MI, Khafagy RM, Hussien MSA, Sakr GB, Ibrahim MA, Yahia IS, Zahran HY (2022) Enhancing the structural, optical, electrical, properties and photocatalytic applications of ZnO/PMMA nanocomposite membranes: towards multifunctional membranes. *J Mater Sci Mater Electron* 33:1977–2002
34. Sengwa RJ, Dhatarwal P (2021) Polymer nanocomposites comprising PMMA matrix and ZnO, SnO₂, and TiO₂ nanofillers: a comparative study of structural, optical, and dielectric properties for multifunctional technological applications. *Opt Mater* 113:110837
35. Zhou Y, Liu Q, Chen F, Sun X, Li S, Guo J, Zhao Y, Yang Y, Xu J (2021) Gradient dielectric constant sandwich-structured BaTiO₃/PMMA nanocomposites with strengthened energy density and ultralow-energy loss. *Ceram Int* 47:5112–51222
36. Muller O, Hege C, Guerchoux M, Merlat L (2022) Synthesis, characterization and nonlinear optical properties of polylactide and PMMA based azophloxine nanocomposites for optical limiting applications. *Mater Sci Eng B* 276:115524
37. Dhatarwal P, Choudhary S, Sengwa RJ (2021) Dielectric and optical properties of alumina and silica nanoparticles dispersed poly(methyl methacrylate) matrix-based nanocomposites for advanced polymer technologies. *J Polym Res* 28:63
38. Dhatarwal P, Sengwa RJ (2020) Tunable β -phase crystals, degree of crystallinity, and dielectric properties of three-phase PVDF/PEO/SiO₂ hybrid polymer nanocomposites. *Mater Res Bull* 129:110901
39. Xia J, Zheng Z, Guo Y (2022) Mechanically and electrically robust, electro-spun PVDF/PMMA blend films for durable triboelectric nanogenerators. *Compos Par A* 157:106914
40. Li Y, Zhang G, Song S, Xu H, Pan M, Zhong GJ (2017) How chain intermixing dictates the polymorphism of PVDF in poly(vinylidene fluoride)/polymethylmethacrylate binary system during recrystallization: a comparative study on core-shell particles and latex blend. *Polymers* 9:448
41. Cui Z, Hassankiadeh NT, Zhuang Y, Drioli E, Lee YM (2015) Crystalline polymorphism in poly(vinylidene fluoride) membranes. *Prog Polym Sci* 51:94–126
42. Meng Q, Li W, Zheng Y, Zhang Z (2010) Effect of poly(methyl methacrylate) addition on the dielectric and energy storage properties of poly(vinylidene fluoride). *J Appl Polym Sci* 116:2674–2684
43. Afonso E, Gómez AM, Tiemblo P, Garcia N (2021) Industrially viable method for producing all-polymer hydrophobic surfaces apt for slippery liquid-infused substrates. *Appl Surf Sci* 535:147728
44. Cai X, Lei T, Sun D, Lin L (2017) A critical analysis of the α , β and γ phases in poly(vinylidene fluoride) using FTIR. *RSC Adv* 7:15382–15389
45. Elashmawi IS, Hakeem NA (2008) Effect of PMMA addition on characterization and morphology of PVDF. *Polym Eng Sci* 48:895–901
46. Satapathy S, Pawar S, Gupta PK, Varma KBR (2011) Effect of annealing on phase transition in poly(vinylidene fluoride) films prepared using polar solvent. *Bull Mater Sci* 34:727
47. Namouchi F, Smaoui H, Fourati N, Zerrouki C, Guermazi H, Bonnet JJ (2009) Investigation on electrical properties of thermally aged PMMA by combined use of FTIR and impedance spectroscopies. *J Alloys Compd* 469:197–202
48. Rai VN, Mukherjee C, Jain B (2017) UV-Vis and FTIR spectroscopy of gamma irradiated polymethylmethacrylate. *Indian J Pure Appl Phys* 55:775–785

49. Veitmann M, Chapron D, Bizet S, Devisme S, Guilment J, Royaud I, Poncot M, Bourson P (2015) Thermal behavior of PVDF/PMMA blends by differential scanning calorimetry and vibrational spectroscopies (Raman and Fourier transform infrared). *Polym Test* 48:120–124
50. Gregorio RG, Nociti NCPDS (1995) Effect of PMMA addition on the solution crystallization of the alpha and beta phases of poly(vinylidene fluoride) (PVDF). *J Phys D* 28:432–436
51. Dhatarwal P, Sengwa RJ (2021) Superior optical and dielectric properties of ultrasonic-assisted solution-cast prepared PMMA/MMT nanocomposite films. *Funct Compos Struct* 3:025008
52. Koseki Y, Aimi K, Ando S (2012) Crystalline structure and molecular mobility of PVDF chains in PVDF/PMMA blend films analysed by solid-state ^{19}F MAS NMR spectroscopy. *Polym J* 44:757–763
53. Mazuki NF, Nagao Y, Kufian MZ, Samsudin AS (2022) The influences of PLA into PMMA on crystallinity and thermal properties enhancement-based hybrid polymer in gel properties. *Mater Today Proc* 49:3105–3111
54. Freire E, Bianchi O, Monteiro EEC, Nunes RCR, Forte MC (2009) Processability of PVDF/PMMA blends studied by torque rheometry. *Mater Sci Eng C* 29:657–661
55. Pawde SM, Deshmukh K (2009) Investigation of the structural, thermal, mechanical, and optical properties of poly(methyl methacrylate) and poly(vinylidene fluoride) blends. *J Appl Polym Sci* 114:2169–2179
56. Zhang Y, Liu Y, Tang C, Yao R, Fan Y, Gao J, Zhong L (2020) Enhanced thermal stability of electrical properties in PVDF/PMMA blend. In: *IEEE conference on electrical insulation dielectric phenomena*, 188–191
57. Lei C, Wang X, Tu D, Wang H, Du Q (2009) Charge distribution in PVDF/PMMA blends under DC field. *Mater Chem Phys* 114:272–278
58. Song H, Yang S, Sun S, Zhang H (2013) Effect of miscibility and crystallization on the mechanical properties and transparency of PVDF/PMMA blends. *Polym Plast Technol Eng* 52:221–227
59. Abaci U, Guney HY, Yilmazoglu M (2021) Plasticizer effect on dielectric properties of poly(methyl methacrylate)/titanium dioxide composites. *Polym Polym Compos* 29:S565–S574
60. Lavina S, Negro E, Pace G, Gross S, Depaoli G, Vidali M, Noto VD (2007) Dielectric low-k composite films based on PMMA, PVC and methylsiloxane-silica: synthesis, characterization and electrical properties. *J Non-Cryst Solids* 353:2878–2888
61. Yu K, Wang H, Zhou Y, Bai Y, Niu Y (2013) Enhanced dielectric properties of BaTiO_3 /poly(vinylidene fluoride) nanocomposites for energy storage applications. *J Appl Phys* 113:034105
62. Wang HQ, Wang JW, Wang XZ, Gao XH, Zhuang GC, Yang JB, Ren H (2022) Dielectric properties and energy storage performance of PVDF-based composites with MoS_2 @MXene nanofiller. *Chem Eng J* 437:135431
63. Feng Y, Deng Q, Peng C, Wu Q (2019) High dielectric and breakdown properties achieved in ternary BaTiO_3 /MXene/PVDF nanocomposites with low-concentration fillers from enhanced interface polarization. *Ceram Int* 45:7923–7930
64. Clark AG, Montero MS, Govinna ND, Lounder SJ, Asatekin A, Cebe P (2020) Relaxation dynamics of blends of PVDF and zwitterionic copolymer by dielectric relaxation spectroscopy. *J Polym Sci* 58:1311–1324
65. Dhatarwal P, Sengwa RJ, Choudhary S (2022) Broadband radio frequency dielectric permittivity and electrical conductivity of dispersed tin oxide and silica nanoparticles in poly(ethylene oxide)/poly(methyl methacrylate) blend matrix-based nanocomposites for nanodielectric applications. *J Macromol Sci B Phys* 61:111–120
66. Sengwa RJ, Dhatarwal P (2022) Thermally improved crystalline phase and intercalated PEO/OMMT nanocomposites for high to ultrahigh radio frequency range low-permittivity nanodielectrics. *J Appl Polym Sci* 139:51599
67. Sengwa RJ, Choudhary S (2014) Dielectric properties and fluctuating relaxation processes of poly(methyl methacrylate) based polymeric nanocomposites electrolytes. *J Phys Chem Solids* 75:765–774
68. Alrooqi A, Al-Amshany ZM, Al-Harbi LM, Altalhi TA, Refat MS, Hassanien AM, Atta AA (2022) Impact of charge transfer complex on the dielectric relaxation processes in poly(methyl methacrylate) polymer. *Molecules* 27:1993
69. Fahmy T, Elzanaty H (2019) AC conductivity and broadband dielectric spectroscopy of a poly(vinyl chloride)/poly(ethyl methacrylate) polymer blend. *Bull Mater Sci* 42:220

Publisher's Note Springer Nature remains neutral with regard to jurisdictional claims in published maps and institutional affiliations.

Springer Nature or its licensor (e.g. a society or other partner) holds exclusive rights to this article under a publishing agreement with the author(s) or other rightsholder(s); author self-archiving of the accepted manuscript version of this article is solely governed by the terms of such publishing agreement and applicable law.